

Supporting Information: Rotational spectroscopy of methyl tert-butyl ether with a new K_a band chirped-pulse Fourier transform microwave spectrometer

Kyle N. Crabtree,^{*,†} J. H. Westerfield,[†] Chisom A. Dim,[†] Kelly S. Meyer,[†]
Sommer L. Johansen,^{†,‡} Zachary S. Buchanan,[†] and Paul A. Stucky[†]

[†]*University of California, Davis, Davis, CA 95616*

[‡]*Present Address: Sandia National Laboratories, Livermore, CA*

E-mail: kncrabtree@ucdavis.edu

List of Figures

S1	K_a -band spectrometer schematic	3
S2	Pulse timing diagram	5
S3	MP2/ANO0 internal rotation potentials	5
S4	MP2/ANO0 V_3 only internal rotation potentials	6
S5	MP2/cc-pVDZ internal rotation potentials	6
S6	MP2/cc-pVDZ V_3 only internal rotation potentials	6
S7	Error in 2D PES fit	7
S8	a -type R-branch rotational bands	7
S9	Isotopologue spectra	9
S10	$^{13}\text{C}4$ isotopologue structure	10

List of Tables

S1	Component list for K_a band CP-FTMW spectrometer.	4
S2	S-reduction centrifugal distortion comparison	8
S3	Contents of fit archive	8
S4	Contents of sims archive	10
S5	Contents of spectra archive	11
S6	Contents of theory archive	12
S7	Contents of xiam archive	13

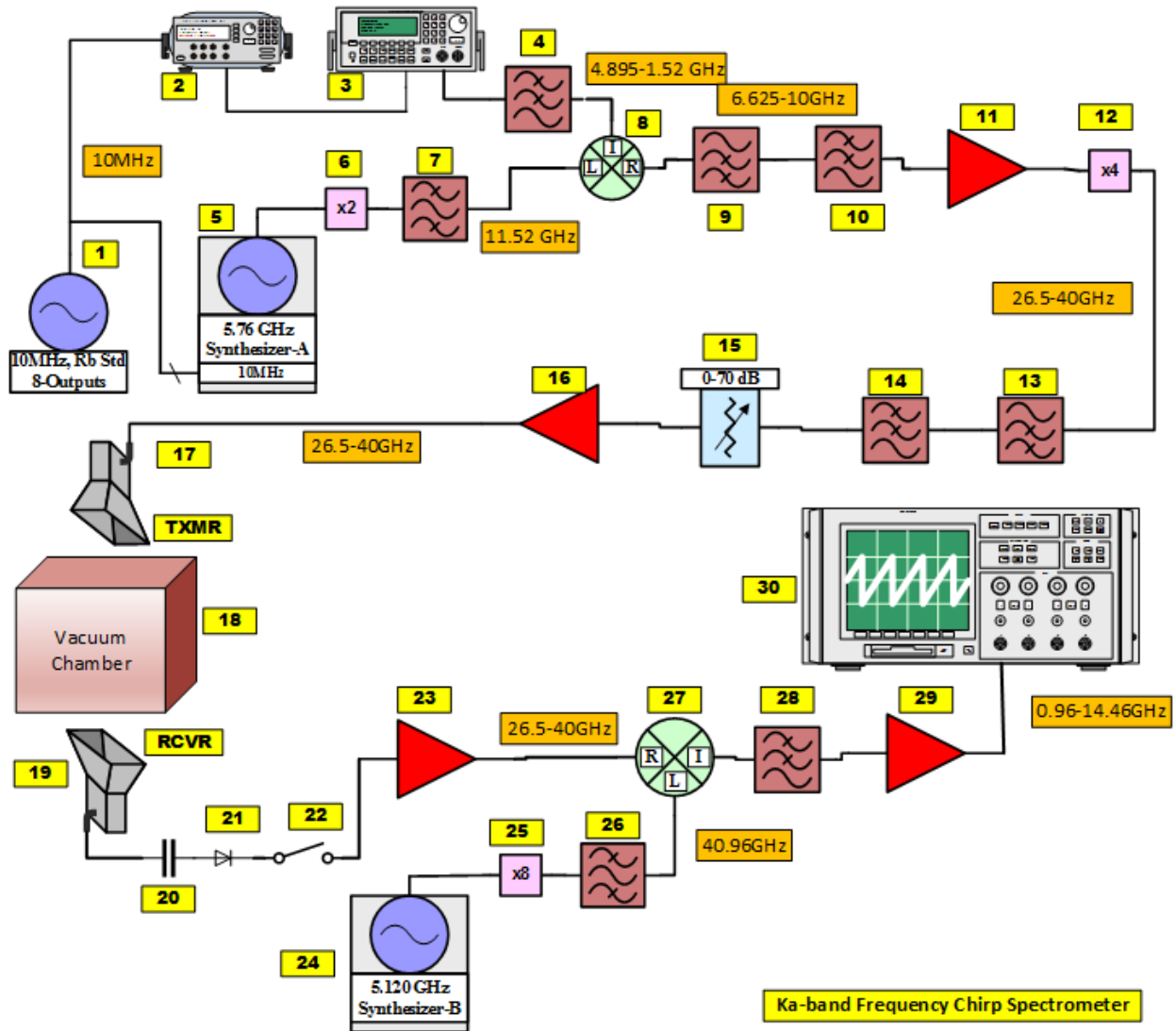


Figure S1: Detailed schematic of K_a band CP-FTMW spectrometer. Numbered components are identified in Table S1.

Table S1: Component list for K_a band CP-FTMW spectrometer.

Number	Manufacturer	Model	Details
1	Stanford Research Systems	FS725	10 MHz Rubidium Frequency Standard, 8 outputs
2	Stanford Research Systems	DG645	Low jitter delay/pulse generator, 4 pulse outputs, <25 ps rms jitter
3	Tektronix	AWG70002A	Arbitrary waveform generator, 2-channel, 8 bits, 16 GSa/s
4	K&L Microwave	6L250-6000/T18000-O/O	Low pass filter, $f_{1dB}=5400$ MHz, IL=0.4 dB, $f_{3dB}=6047$ MHz
5,24	Valon Technology	5009	Dual independent synthesizer, 6 GHz, +15 dBm
6	Wright Technologies	ASX13-220	Active freq. doubler, $f_{out}=10.5-12.5$ GHz, $(P_{in}, P_{out})=(+10,+20)$ dBm
7	K&L Microwave	6C52-11520/T200-O/O	Band pass filter, $f_c=11527$ MHz, IL=1.18 dB, BW=239 MHz
8	Marki Microwave	T3H-18IS	Triple balanced mixer, (RF,LO,IF)=0.01-18 GHz, CL=9.5 dB
9	K&L Microwave	8L250-10200/T30000-O/OP	Low pass filter, $f_{3dB}=10438$ MHz, IL=0.57 dB@10 GHz
10	Mini-Circuits	VHF-6010+	High pass filter, $f_{3dB}=6010$ MHz
11	Miteq	AFSD5-060120-30-26P	Amplifier, BW=6-12 GHz, G=26 dB, $P_{1dB}=26$ dBm, NF=3 dB
12	Wright Technologies	ASX40-420	Active freq. quadrupler, $f_{out}=26-40$ GHz, $(P_{in}, P_{out})=(+10,+20)$ dBm
13	AMTI	H26G40G1	High pass filter, $f_{3dB}=25$ GHz, Pass Band=26-40 GHz, IL<1 dB
14	Marki Microwave	FLP-4300	Low pass filter, $f_{3dB}=43$ GHz, IL<2 dB
15	Agilent	84907L	Step attenuator, BW=DC-40 GHz, 0 to 70 dB, 10 dB steps, with switch controller
16	Applied Systems Engineering	187Ka-H	Amplifier, TWT, BW=26.5-40 GHz, $P_{sat}=170$ W, Max Pulse Width=100 μ s, PRF _{max} =100 kHz, $\tau_r=15$ ns
17,19	Advanced Technical Materials	PNR 28-449-6/24	Rectangular horn antenna, BW=26.5-40 GHz, G=25 dBi, includes coax-wg adptr, kapton window
18	Vacuum Chamber	—	Eccosorb-lined (microwave absorber) stainless steel ISO-400 6-way cross
20	Tektronix	PSPL5509	DC block, BW=7 kHz-50 GHz, IL=1 dB@40 GHz, $\tau_r=5$ ps
21	Clear Microwave	LT1840H	Power limiter, BW=18-40 GHz, IL=4.2 dB max, $P_{leak}=21$ dBm, $(P_{cw}, P_{peak})=(1,100)$ W
22	Quinstar	QSC-ASR000	Coaxial SPST PIN switch, BW=26.5-40 GHz, IL=2.5 dB, Iso=28 dB, $P_{max}=30$ dBm, $\tau=5$ ns
23	Miteq	AMF-6F-26004000-25-13P	Amplifier, BW=26-40 GHz, G=40 dB, $P_{1dB}=15$ dBm, NF=3.5 dB
25	Wright Technologies	APS15-0191	Active freq. multiplier, x8, $f_{out}=40.5-41.5$ GHz, $(P_{in}, P_{out})=(+12,+20)$ dBm
26	Eastern Wireless	EWT-31-0351	Band pass filter, $f_c=41$ GHz, BW=292 MHz, IL=1.4 dB, RL=17.4 dB
27	Marki Microwave	ML1-1644IS	Double-balanced mixer, (RF,LO)=16-44 GHz, IF=DC-21 GHz, CL=7 dB, $P_{1dB}=9$ dBm
28	Marki Microwave	FLP-1740	Low pass filter, $f_{3dB}=17.4$ GHz, IL<0.9 dB
29	Mini-Circuits	ZVA-183-S+	Amplifier, BW=0.7-18 GHz, G=26 dB, $P_{1dB}=24$ dBm, NF=3 dB
30	Tektronix	DSA71604C	Oscilloscope, BW=DC-16 GHz, 4 Ch, Max Sample Rate=100 GS/s

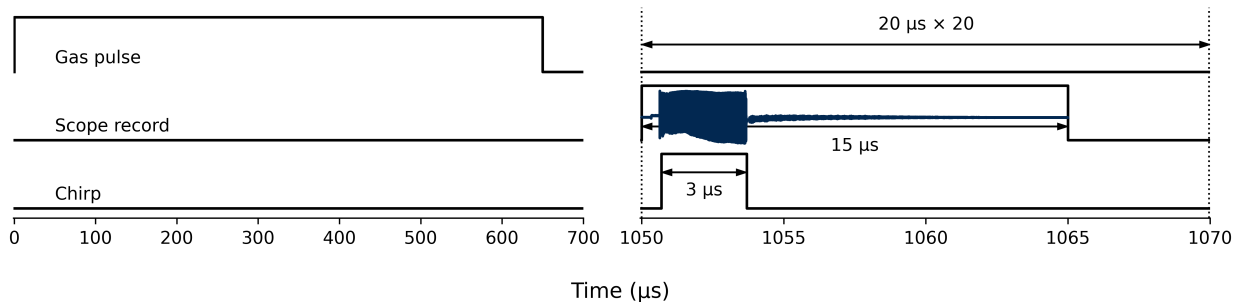


Figure S2: Pulse timing diagram.

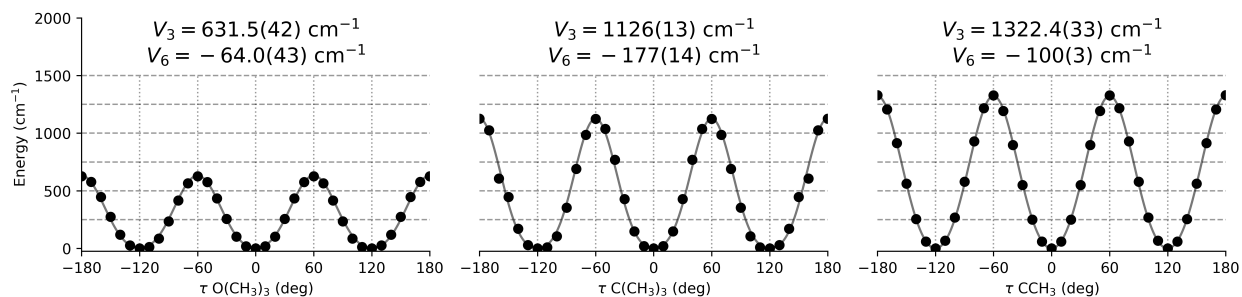


Figure S3: MP2/ANO0 potential barriers for the internal rotations of MTBE (points), along with fits (lines). Angles are defined such that $\tau = 0$ at the equilibrium geometry: i.e., $\tau \text{ OCH}_3 = (\tau \text{ H}_6\text{C}_0\text{O}_1\text{C}_2 - 180^\circ)$. Values in parentheses are 1σ uncertainties in the fit parameters.

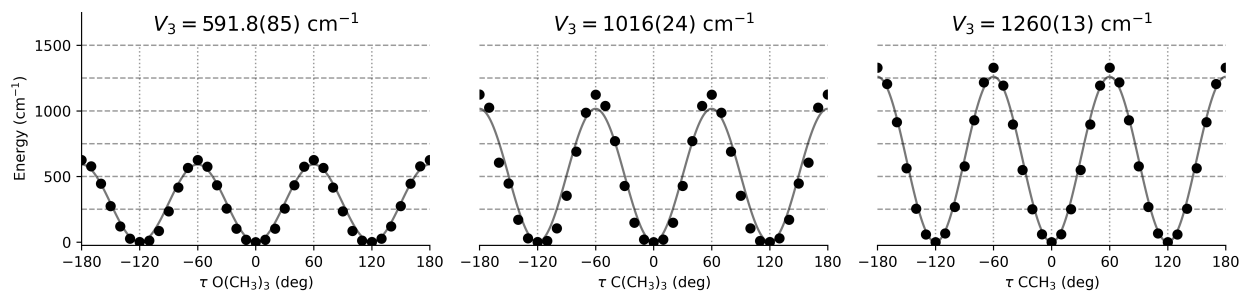


Figure S4: MP2/ANO0 internal rotation potentials for MTBE with a V_3 -only fit.

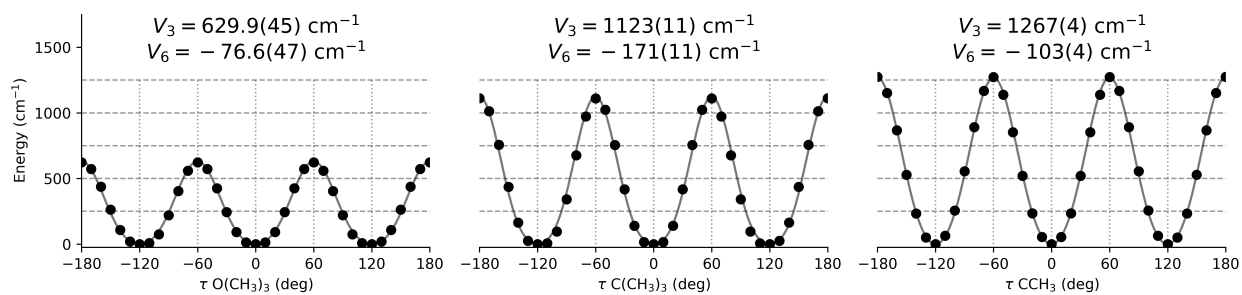


Figure S5: MP2/cc-pVDZ internal rotation potentials for MTBE.

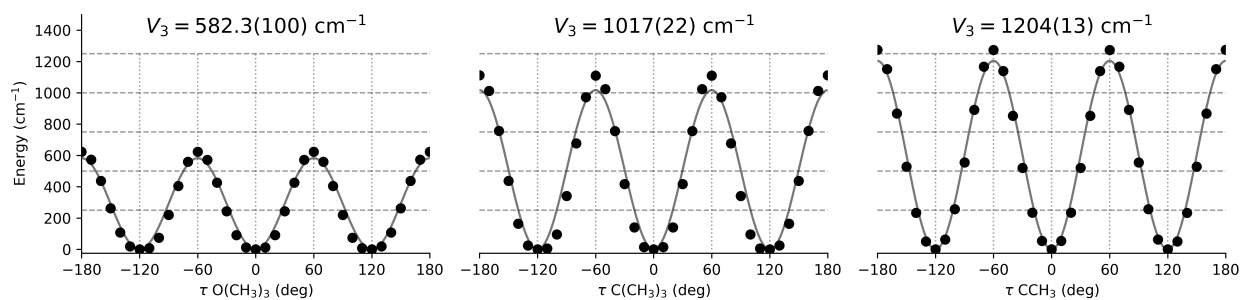


Figure S6: MP2/cc-pVDZ internal rotation potentials for MTBE with a V_3 -only fit.

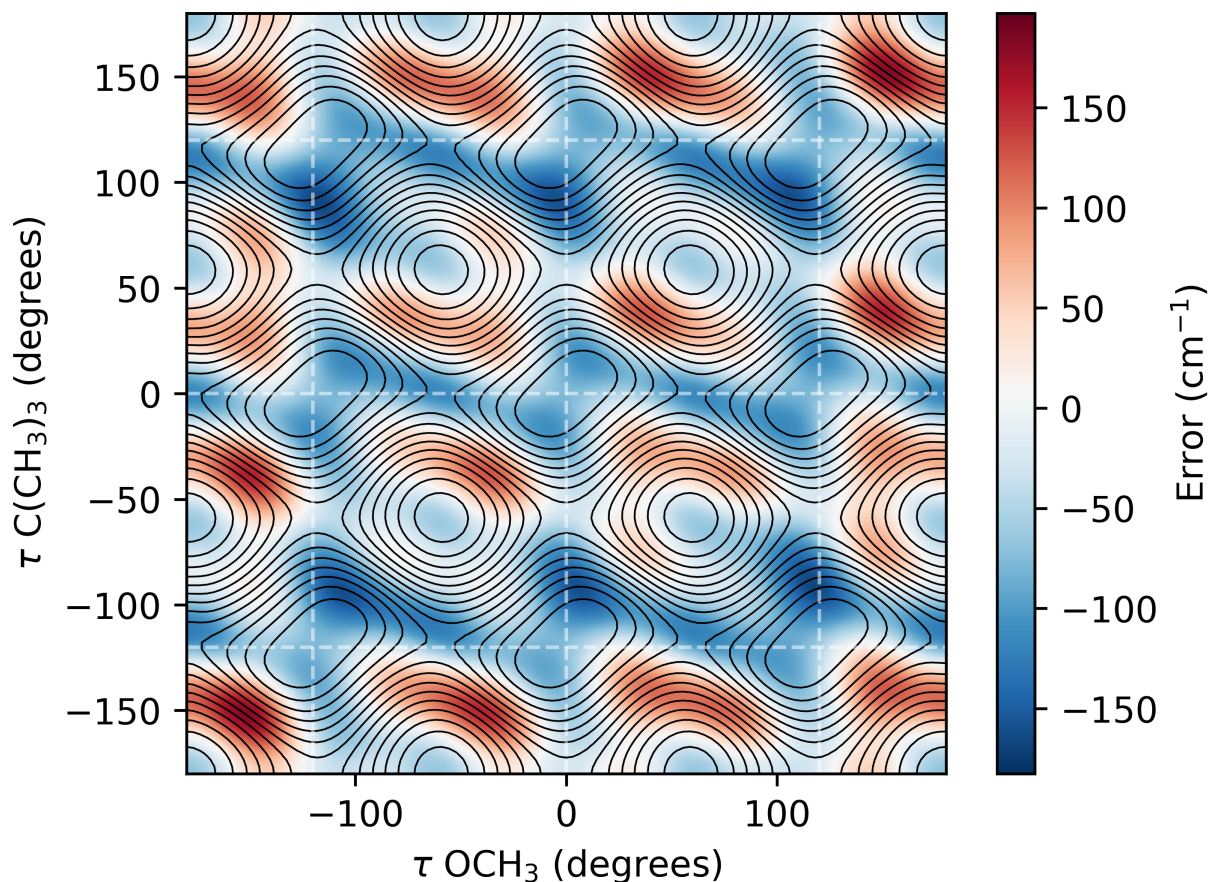


Figure S7: Error in the fit to the 2D MP2/cc-pVDZ PES of MTBE for the coupled rotation of the OCH₃ and C(CH₃)₃ groups shown in Table 4 of the main text. Contours show the potential energy and are drawn at 150 cm⁻¹ intervals, and the dashed gray lines show angles of 0 and $\pm 120^\circ$.

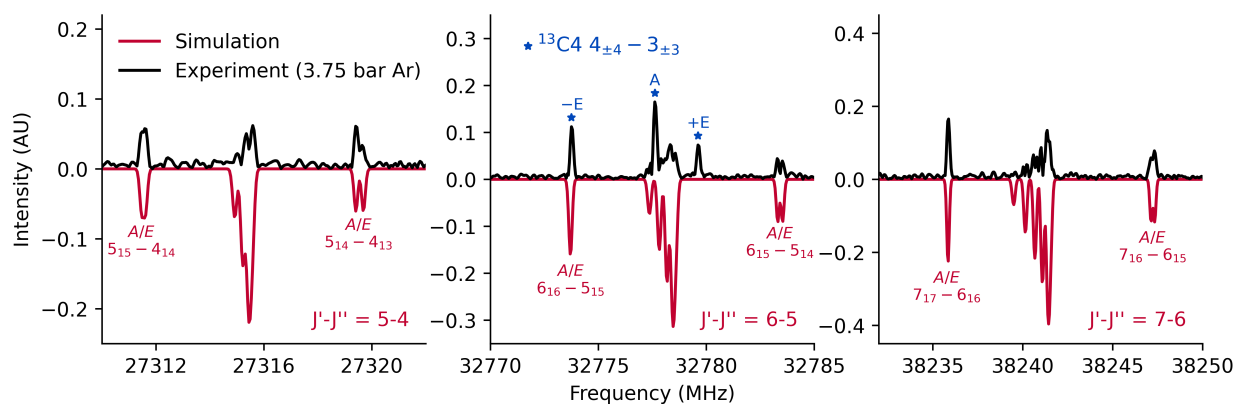


Figure S8: Three *a*-type R-branch rotational bands. Experimental intensities within the cluster of $K_a \neq 1$ overlapped transitions are attenuated likely due to frequency-dependent phase shifts, while the intensity agreement for the more isolated $K_a = 1$ transitions is considerably better. A triplet arising from the ¹³C4 isotopologue is also visible in this region.

Table S2: Comparison of calculated centrifugal distortion terms (S-reduction, I^r representation) with experimentally fitted values.

Parameter	MP2/cc-pVDZ	MP2/ANO0	B3LYP/6-311+G(2d,p)	Experiment
ω_{tBu} (cm^{-1})	18.	32.	58.	--
D_J (kHz)	0.354	0.336	0.329	0.32352(51)
D_{JK} (kHz)	47.9	15.8	5.09	4.212900(13)
D_K (kHz)	-47.5	-15.7	-4.53	-3.65752(55)
d_1 (kHz)	-0.00791	-0.00837	-0.00684	-0.00512(37)
d_2 (kHz)	0.00729	-0.00309	-0.00800	-0.0118(12)
H_J (Hz)	0.0021	0.00029	0.000048	[0.000048]
H_{JK} (Hz)	3.12	0.316	0.0269	0.01096(4)
H_{KJ} (Hz)	-6.96	-0.690	-0.0571	-0.0174(7)
H_K (Hz)	3.84	0.374	0.0304	[0.0304]
h_1 (Hz)	-0.00014	0.000016	0.000016	[0.000016]
h_2 (Hz)	-0.00103	-0.000120	0.0000005	[0.0000005]
h_3 (Hz)	0.00014	-0.000015	-0.000014	[-0.000014]

Table S3: Filenames and descriptions contained within the fit directory of the data archive file. Each xi file contains the linelist for the respective species, and the xo file contains fitted parameters and deviations of the transition frequencies.

Filename	Description
mtbe-13c0-s.xi	$^{13}\text{C}_0$ isotopologue, S reduction, XIAM input file
mtbe-13c0-s.xo	$^{13}\text{C}_0$ isotopologue, S reduction, XIAM output file
mtbe-13c2-s.xi	$^{13}\text{C}_2$ isotopologue, S reduction, XIAM input file
mtbe-13c2-s.xo	$^{13}\text{C}_2$ isotopologue, S reduction, XIAM output file
mtbe-13c3-s.xi	$^{13}\text{C}_3$ isotopologue, S reduction, XIAM input file
mtbe-13c3-s.xo	$^{13}\text{C}_3$ isotopologue, S reduction, XIAM output file
mtbe-13c4-s.xi	$^{13}\text{C}_4$ isotopologue, S reduction, XIAM input file
mtbe-13c4-s.xo	$^{13}\text{C}_4$ isotopologue, S reduction, XIAM output file
mtbe-18o-s.xi	^{18}O isotopologue, S reduction, XIAM input file
mtbe-18o-s.xo	^{18}O isotopologue, S reduction, XIAM output file
mtbe-gs-a.xi	MTBE parent, A reduction, Ground state XIAM input file
mtbe-gs-a.xo	MTBE parent, A reduction, Ground state XIAM output file
mtbe-gs-s.xi	MTBE parent, S reduction, Ground state XIAM input file
mtbe-gs-s.xo	MTBE parent, S reduction, Ground state XIAM output file
mtbe-vib-s.xi	MTBE parent, S reduction, Two state XIAM input file
mtbe-vib-s.xo	MTBE parent, S reduction, Two state XIAM output file
mtbe.stf	Input file for STRFIT program, r_0 structure
mtbe.out	Output file for STRFIT program, r_0 structure

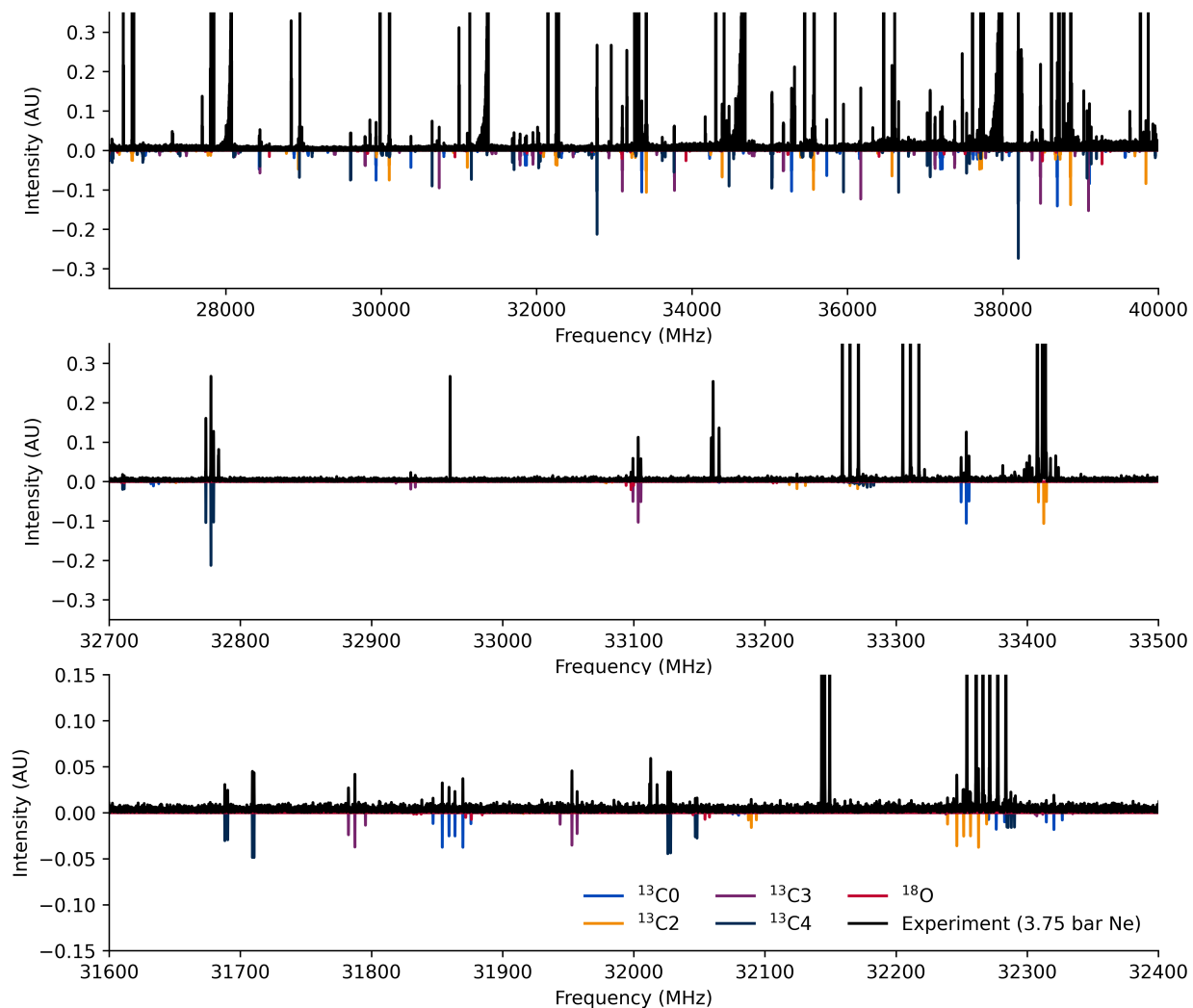


Figure S9: K_a band spectrum of MTBE with a backing pressure of 3.75 bar Ne (black), along with simulated spectra for each heavy atom isotopologue. The simulated spectra are based on fit parameters shown in Table 7 and a rotational temperature of 7 K. The center panel shows a portion of the spectrum highlighting transitions with $K_a \geq 3$ where the $^{13}\text{C4}$ isotopologue transitions are twice as strong as those of the other ^{13}C isotopologues. The bottom panel shows a region of low- K_a transitions where the transition intensities are roughly equal owing to the $\sqrt{2}$ decrease in dipole moment canceling the factor of 2 increase from the two equivalent substitution sites.

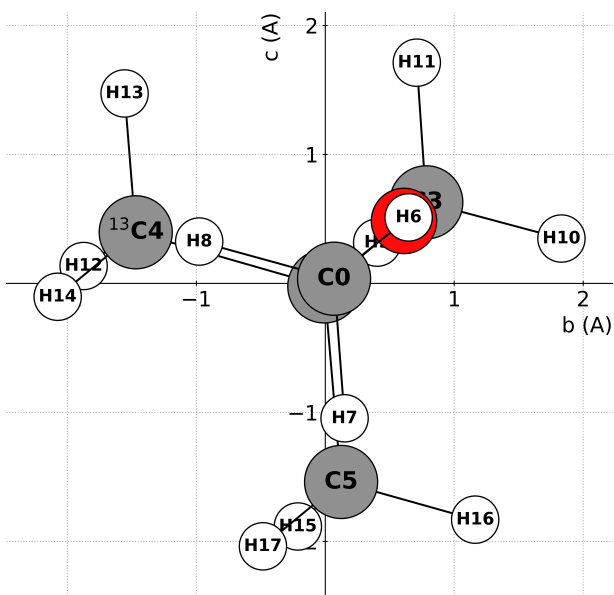


Figure S10: Orientation of the b and c inertial axes for the off-axis substituted $^{13}\text{C}_4$ isotopologue.

Table S4: Filenames and descriptions contained within the sims directory of the data archive file. Each xi file contains the parameters used to generate the simulation, and the corresponding xo file contains the simulated transition frequencies and intensities for the indicated species.

Filename	Description
13c0-7k.xi	$^{13}\text{C}_0$ isotopologue 7 K simulation XIAM input file
13c0-7k.xo	$^{13}\text{C}_0$ isotopologue 7 K simulation XIAM output file
13c2-7k.xi	$^{13}\text{C}_2$ isotopologue 7 K simulation XIAM input file
13c2-7k.xo	$^{13}\text{C}_2$ isotopologue 7 K simulation XIAM output file
13c3-7k.xi	$^{13}\text{C}_3$ isotopologue 7 K simulation XIAM input file
13c3-7k.xo	$^{13}\text{C}_3$ isotopologue 7 K simulation XIAM output file
13c4-7k.xi	$^{13}\text{C}_4$ isotopologue 7 K simulation XIAM input file
13c4-7k.xo	$^{13}\text{C}_4$ isotopologue 7 K simulation XIAM output file
18o-7k.xi	^{18}O isotopologue 7 K simulation XIAM input file
18o-7k.xo	^{18}O isotopologue 7 K simulation XIAM output file
mtbe-7k.xi	MTBE two-state 7 K simulation XIAM input file
mtbe-7k.xo	MTBE two-state 7 K simulation XIAM output file
mtbe-20k.xi	MTBE two-state 20 K simulation XIAM input file
mtbe-20k.xo	MTBE two-state 20 K simulation XIAM output file
mtbe-45k.xi	MTBE two-state 45 K simulation XIAM input file
mtbe-45k.xo	MTBE two-state 45 K simulation XIAM output file
mtbe-ir.xi	MTBE two-state 45 K simulation, I^r representation XIAM input file
mtbe-ir.xo	MTBE two-state 45 K simulation, I^r representation XIAM output file

Table S5: Filenames and descriptions contained within the spectra directory of the data archive file. Directories contain raw data from the Blackchirp program. The csv files contain the numerical values of the free induction decay and Fourier transform data. A python script is provided for processing the raw data to generate the csv files.

Filename	Description
360	Raw data files for Ar, 3.75 bar MTBE spectrum
363	Raw data files for Ar, 1 bar MTBE spectrum
1231	Raw data files for Ne, 3.75 bar MTBE spectrum (Acquisition 1/7)
1242	Raw data files for Ne, 3.75 bar MTBE spectrum (Acquisition 2/7)
1243	Raw data files for Ne, 3.75 bar MTBE spectrum (Acquisition 3/7)
1244	Raw data files for Ne, 3.75 bar MTBE spectrum (Acquisition 4/7)
1245	Raw data files for Ne, 3.75 bar MTBE spectrum (Acquisition 5/7)
1252	Raw data files for Ne, 3.75 bar MTBE spectrum (Acquisition 6/7)
1254	Raw data files for Ne, 3.75 bar MTBE spectrum (Acquisition 7/7)
mtbe-ar-0psi-fid.csv	Processed free induction decay for Ar, 1 bar MTBE spectrum
mtbe-ar-0psi-ft-hann.csv	Processed Fourier transform for Ar, 1 bar MTBE spectrum
mtbe-ar-40psi-fid.csv	Processed free induction decay for Ar, 3.75 bar MTBE spectrum
mtbe-ar-40psi-ft-hann.csv	Processed Fourier transform for Ar, 3.75 bar MTBE spectrum
mtbe-ne-40psi-fid.csv	Processed free induction decay for Ne, 3.75 bar MTBE spectrum
mtbe-ne-40psi-ft-hann.csv	Processed Fourier transform for Ne, 3.75 bar MTBE spectrum
process.py	Python script for generating processed data from raw data files

Table S6: Filenames and descriptions contained within the theory directory of the data archive file. This archive contains output files from quantum chemical calculations, structures, and rotational spectroscopy parameters derived from theoretical structures.

Filename	Description
mtbe-b3lyp.log	B3LYP/6-311+G)2d,p) Geometry optimization and VPT2 calculation
ccsdt-pvtz/geo.xyz	Cartesian coordinates (Å) of the MTBE CCSD(T)/cc-pVTZ geometry
ccsdt-pvtz/iso.csv	Rotational constants and OCH ₃ internal rotation parameters for MTBE isotopologues based on the CCSD(T)/cc-pVTZ optimized geometry
ccsdt-pvtz/moments.csv	Rotational constants and OCH ₃ internal rotation parameters for MTBE based on the CCSD(T)/cc-pVTZ optimized geometry
ccsdt-pvtz/opt.txt	CFOUR CCSD(T)/cc-pVTZ geometry optimization output for MTBE
ccsdt-pvtz/tbu-moments.csv	Rotational constants and C(CH ₃) ₃ internal rotation parameters for MTBE based on the CCSD(T)/cc-pVTZ optimized geometry
mp2-ano0/cch3_ip-1d.xyz	GeomeTRIC output: energies and optimized structures for MP2/cc-ANO0 in-plane CCH ₃ internal rotation potential energy scan
mp2-ano0/geo.xyz	Cartesian coordinates (Å) of the MTBE MP2/cc-ANO0 geometry
mp2-ano0/iso.csv	Rotational constants and OCH ₃ internal rotation parameters for MTBE isotopologues based on the MP2/cc-ANO0 optimized geometry
mp2-ano0/moments.csv	Rotational constants and OCH ₃ internal rotation parameters for MTBE based on the MP2/cc-ANO0 optimized geometry
mp2-ano0/och3-1d.xyz	GeomeTRIC output: energies and optimized structures for MP2/cc-ANO0 OCH ₃ internal rotation potential energy scan
mp2-ano0/opt.txt	CFOUR MP2/cc-ANO0 geometry optimization output for MTBE
mp2-ano0/tbu-1d.xyz	GeomeTRIC output: energies and optimized structures for MP2/cc-ANO0 C(CH ₃) ₃ internal rotation potential energy scan
mp2-ano0/tbu-moments.csv	Rotational constants and C(CH ₃) ₃ internal rotation parameters for MTBE based on the MP2/cc-ANO0 optimized geometry
mp2-ano0/vibrot.txt	CFOUR output from MP2/cc-ANO0 vibration-rotation interaction calculations
mp2-pvdz/cch3_ip-1d.xyz	GeomeTRIC output: energies and optimized structures for MP2/cc-pVDZ in-plane CCH ₃ internal rotation potential energy scan
mp2-pvdz/geo.xyz	Cartesian coordinates (Å) of the MTBE MP2/cc-pVDZ geometry
mp2-pvdz/iso.csv	Rotational constants and OCH ₃ internal rotation parameters for MTBE isotopologues based on the MP2/cc-pVDZ optimized geometry
mp2-pvdz/moments.csv	Rotational constants and OCH ₃ internal rotation parameters for MTBE based on the MP2/cc-pVDZ optimized geometry
mp2-pvdz/och3-1d.xyz	GeomeTRIC output: energies and optimized structures for MP2/cc-pVDZ OCH ₃ internal rotation potential energy scan
mp2-pvdz/och3-tbu-2d.xyz	GeomeTRIC output: energies and optimized structures for MP2/cc-pVDZ OCH ₃ /C(CH ₃) ₃ 2D internal rotation potential energy scan
mp2-pvdz/opt.txt	CFOUR MP2/cc-pVDZ geometry optimization output for MTBE
mp2-pvdz/tbu-1d.xyz	GeomeTRIC output: energies and optimized structures for MP2/cc-pVDZ C(CH ₃) ₃ internal rotation potential energy scan
mp2-pvdz/tbu-moments.csv	Rotational constants and C(CH ₃) ₃ internal rotation parameters for MTBE based on the MP2/cc-pVDZ optimized geometry
mp2-pvdz/vpt2.txt	CFOUR output from MP2/cc-pVDZ VPT2 calculations

Table S7: Filenames and descriptions contained within the xiam directory of the data archive file. This archive contains the modified Fortran files used to change the display of the intensity and error values in the XIAM output files.

Filename	Description
iamint.f	Modified file implementing scientific notation in intensity output
iamio.f	Modified file implementing additional digits in line error output